Performance of the Drift Tubes for the Barrel Muon Chambers of the CMS Detector at LHC

Ivano Lippi [a] for the CMS Barrel Muon Group

[a]I.N.F.N. Sezione di Padova and Dipartimento di Fisica Università di Padova
Via Marzolo 8, I-35131 Padova, Italy

The barrel muon chambers of the CMS experiment are made assembling quadruplets of 4 layers of rectangular drift tubes. We present the performance of a prototype of such quadruplets exposed at a muon beam. Characteristics as noise, efficiency, drift velocity and resolution, are studied for various data taking conditions, as well as the effects of the magnetic field. A special emphasis is given to the performance aspects related to the trigger capability of the chambers.

1. Introduction

The barrel muon detector of the CMS experiment [1] is devoted to the muons tracks identification, measurement and triggering, the latter being the most demanding feature required. The detector chosen by the CMS collaboration is based on 4 layers of arrays of rectangular drift tubes.

The performance of a prototype of such detector has been studied with a muon test beam. The present prototype is an evolution of previous ones of the same kind, whose performance results have already been published [2,3].

This completely revised version, with new cell structure, material and construction technique, which reached the final configuration envisaged for the CMS detector, led us to renew the performance studies. Furthermore, for the first time the effects of the magnetic field on the performance have been studied.

2. Detector Description

The barrel muon detector of the CMS experiment is made by 4 cylindrical stations placed around the solenoidal magnetic field, into the iron return yoke of the magnet.

The barrel, 13.5 meters long, is divided into 5 wheels, each one divided into 12 azimuthal sectors, thus giving a total of 240 chambers, whose arrangement can be seen in fig. 1, which shows a schematic transverse view of two sectors of one of the wheels.

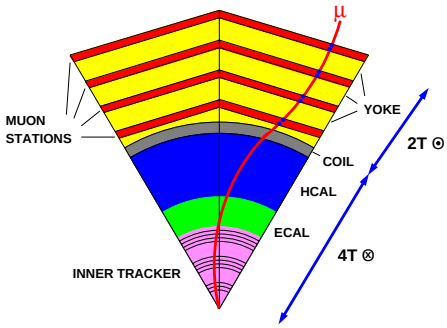

Figure 1. Schematic transverse view of two sectors of a wheel of the CMS detector

The chambers are 2.5 meters long, with a variable width between 2 and 4 meters from the internal to the external stations, and 29 cm thick.

The fundamental component of the chamber is the quadruplet, 4 layers of rectangular drift cells staggered by half cell. Each chamber is made of 3 quadruplets, the two external ones have the wires parallel to the beam line and are devoted to the measurement of the track in the bending plane, the internal one has the wires orthogonal to the beam line and is devoted to the measurement into the longitudinal plane.

The three quadruplets are glued to an aluminium honeycomb plate, to reach the required overall stiffness.

Every quadruplet is made by 5 aluminium foils 2 mm thick, and the cell structure is built by the insertion of aluminium I-beams, of 10 mm height.

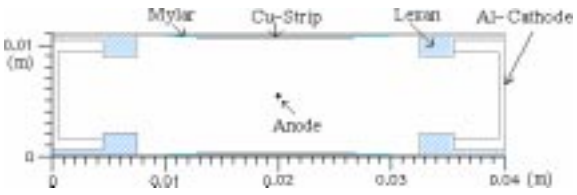

Figure 2. Transverse view of a Cell

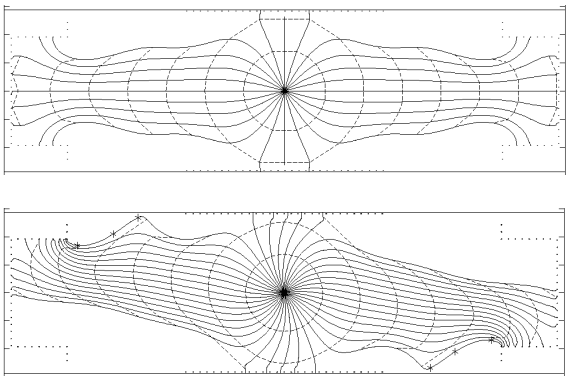

Figure 3. Drift lines of a cell as calculated by the program GARFIELD. Below are the drift lines as distorted by a magnetic fileld parallel to the wires

The drift cell, shown in fig. 2, has a rectangular section of 4.0×1.3 cm^2. The anode is a central stainless steel wire of 50 μm of diameter, the cathodes are the I-beams of the cells structure, isolated from the grounded aluminium planes by a polycarbonate (Lexan) strip, 0.5 mm thick. A field shaping electrode facing the wires is added in form of copper strips 14 mm wide, in order to improve the field uniformity, and therefore the linearity of the space-time relation through a saturated drift velocity.

The behaviour of the cell have been simulated with the program GARFIELD [4]. In fig. 3 are shown the drift lines calculated by the program for the reference voltage settings and the distorsion effect on them of a magnetic field parallel to the wires.

Every station will have to provide in the bending plane, for each crossing track, a track segment with the precision of 100 μm and 1 mrad respectively for the position and the incident angle determination, while for the longitudinal plane the requirements are more relaxed. Given the dimensions and the structure of the chambers, it turns out that the required single cell resolution must be around 250 μm or better.

For the triggering purpose, every muon station will have to identify the bunch crossing at which the muon have been produced, LHC will have a bunch crossing each 25 ns, and a rough estimate of the position and the incident angle, to allow the central trigger processor to perform a momentum cut.

The trigger is performed by each quadruplet using the mean timer technique, already described in [2].

3. Experimental Setup

The prototype is a reduced in size version of the quadruplet, made by four layers of 16 drift tubes each, 1 meter long. It was built in Padova by the Bologna and Padova groups.

The prototype was exposed at the CERN-SpS muon beam of energy 200-300 GeV of the H2 test beam area in August 1995.

The gas mixture used was Ar(85%) and CO_2(15%).

The signal extracted from the wires was processed through the ASD-8 amplifier-shaper-discriminator chip [5], operated with thresholds in the range 1 – 8 fC, the reference value being 4 fC. The output signal was then translated and driven by a dedicated circuit with $\sim$ 100 ns shaping time, and readout by the 32-channels, multihit, 1 ns resolution, LeCroy-2277 TDC, operated in *common stop* mode.

The chamber was operated at different voltage

settings, always with $V_{strip} = -V_{cathode}$, the reference values being

$V_{wire} = 3600\,V$

$V_{strip} = 1800\,V$

$V_{cathode} = -1800\,V$

In the following we will use the notation :

$V_{ampl} = V_{wire} - V_{strip}$

$V_{drift} = V_{strip} - V_{cathode}$

Unless otherwise stated, the voltages and threshold settings are at the reference values.

The chamber was placed on a mechanical structure which allowed to rotate it around an horizontal axis, to take data with various angles of incidence of the tracks, and was placed inside a uniform magnetic field parallel to the beam direction, varying in the range 0 – 1.5 T, so that rotating the chamber was possible to have components parallel and orthogonal to the wires.

4. Random Noise

Random hits generated by noise in the cell could affect the track identification and the trigger capability of the chambers, producing wrong tracks associations and ghost track triggers.

The noise rate has been measured using the multi-hit capability of the TDC and its full 64 μs active time range. The physical hits due to the particles crossing are limited to a restricted time range (TDC time $< 2.1\ \mu$s), due to the common stop mode of operation of the TDC's. The number of hits recorded outside this physical range, cell by cell, are counted to evaluate the noise rate. It results in the range 10 – 20 Hz/m, therefore the probability of a random hit occurring in the total drift time of 350 ns, at the expected LHC rate which is about 1 kHz per channel, is below 2%.

5. Feedback Photons

These are the signals generated by electrons extracted from the cathode by photons produced during the multiplication process. These signals are correlated in time to the physical hits and are produced at a fixed delay time, equal to the maximum drift time, thus generating a systematic noise.

From the time difference of the double hits

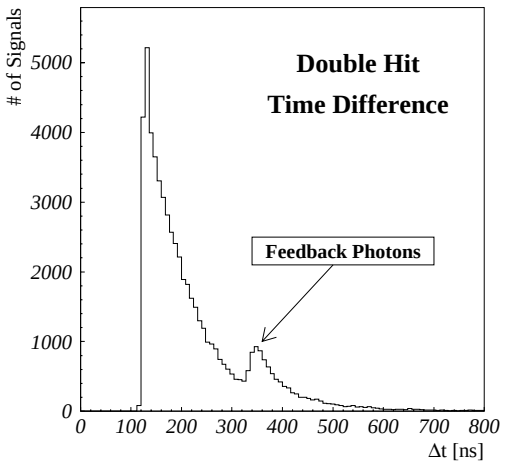

Figure 4. Distribution of the time difference between the first and the second hit for two hits cell signals

events shown in fig. 4, the effect of the feedback photons is evidenced by the bump over the exponential distribution at the expected time difference value.

Its contribution to the noise can be estimated in the range 0.5 – 0.8 % of the total number of physical hits.

6. Efficiency

The efficiency has been calculated for each half-cell, using tracks incident orthogonally to the chamber. The method used provides the efficiency definition.

A sample of events with clean three hits isolated tracks is selected : the events must have one hit per plane, excluding the plane with the half-cell for which the efficiency is calculated, and the three hits must fit a straight line with residuals less then 2.5 σ.

The interpolation/extrapolation provides the definition of the position of the track inside the considered half-cell, in 1 mm bins. The efficiency is then calculated for each bin in the track position, asking for a hit in the half-cell with a physical drift time, and then averaged over the posi-

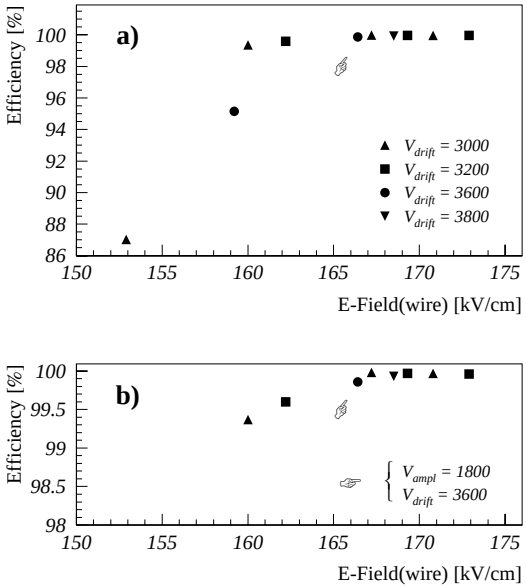

Figure 5. (a) Intrinsic cell efficiency as a function of the electric field on the wire with (b) an enlarged view

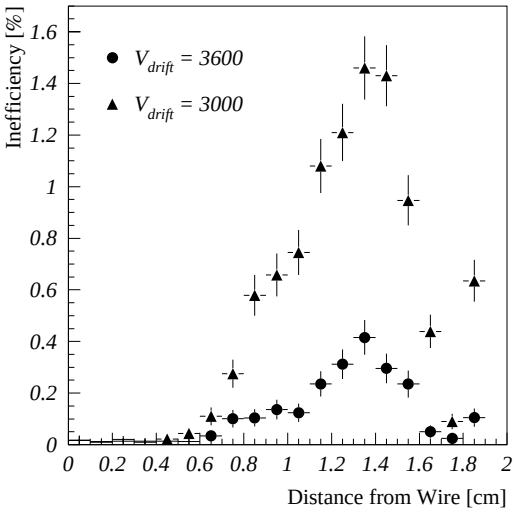

Figure 6. Intrinsic cell inefficiency as a function of the crossing position of the track for two voltages settings

tion bins, thus allowing to evaluate the intrinsic efficiency of the cell, excluding the geometrical acceptance and the systematic effects due to possible non-uniformity inside the cell.

Fig. 5a shows the mean intrinsic cell efficiency, with an enlarged view in fig. 5b. The efficiency is plotted against the value of the electric field on the wire, which is the significant variable for this purpose, as can be seen from the fact that the values measured at different voltages settings lie on the same curve.

The value of the electric field on the wire has been calculated through the program GARFIELD, and results related to the voltages settings by the relation (with V in Volts)

$$E_{wire}\,[V/cm] \;=\; 73.71\,(\,V_{ampl} \;+\; .13\,V_{drift}\,)$$

The inefficiency is very low, 0.2% for the reference voltages $V_{ampl} = 1800$ V and $V_{drift} = 3600$ V, nevertheless it is important to verify if such inefficiency is concentrated into a particular region of the cell, where the value can be much larger. This is in fact the case, as shown in fig. 6, where the inefficiency is plotted as a function of the position of the track.

This small inefficiency can be attributed to the less effective track length available for the production of the ionization clusters in the cell region where the electric field has the largest values, as can be seen from the drift lines shown in fig. 3. Such effect is confirmed by the plots in figg. 7a and 7b, where the efficiency for different values of the incident angle on the transverse plane are shown, and the small inefficiency disappears as the angle of incidence makes the available effective track length larger.

Exactly the same behaviour is observed for tracks with an incident angle on the longitudinal plane, so we can conclude that although a very small intrinsic inefficiency of the cell is present, negligible by itself, it has no effect, given the wide range of angle of incidence of the tracks in CMS.

The efficiency have been studied also varying the threshold applied to the signal. As shown in fig. 7c, there are no significant effects.

The effects of the magnetic field to the efficiency are shown in fig. 8. While a magnetic field

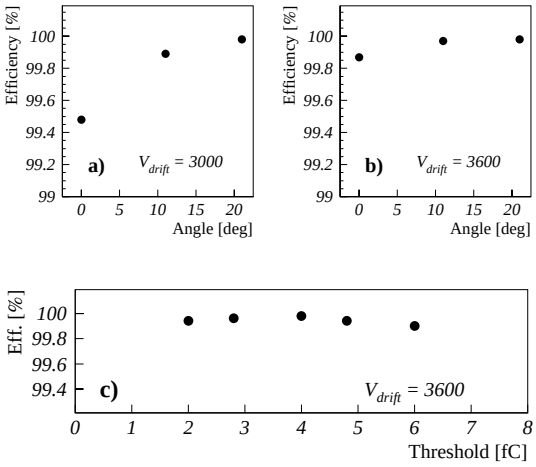

Figure 7. Effect on the intrinsic cell efficiency of the incident angles (a,b) and the threshold (c)

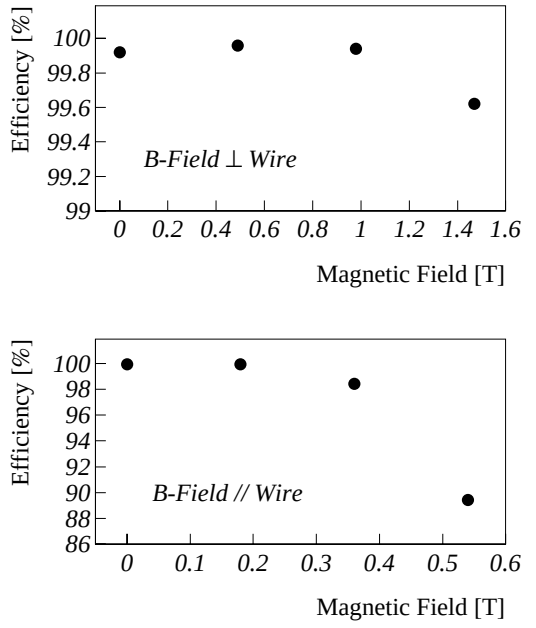

Figure 8. Intrinsic cell efficiency as a function of the magnetic field (a) orthogonal to the wire and (b) parallel to the wire

orthogonal to the wires has no or very little effects on the efficiency, even for values as large as 1.5 T, a component along the wire causes a sizeable drop in the efficiency which could be of the order of 10% for values larger then 0.3 T.

7. δ-rays

The δ-rays production is a significant source of inefficiency, as it strongly affects the track measurement and triggering, spoiling the correlation between the drift time and the track position, as shown as an example in fig. 9 for time t_3.

The δ-rays production effect have been measured using the variables MT_2 and MT_3, defined from fig. 9 as :

$$MT_j = (t_{j-1} + t_{j+1})/2 + t_j$$

The two variables, plotted one against the other, exhibits a strong correlation, as shown in fig. 10. The blob around the maximum drift time value is due to tracks with the measurements not affected by δ-rays production, while if a single drift time measurement is affected, the point lies along one of the four lines clearly visible in the picture, depending on the affected layer.

A track measurement is considered affected by a δ-ray if one or both the variables MT_2 and MT_3 are more then 2.5 σ from their mean value. With the above definition, the different contributions have been computed, and the results are displayed in table 1.

Table 1
δ-rays effects as percentage of tracks affected in 0, 1 or >1 drift time measurements

Not affected		80.8 %
Layer 1	3.4 %	
Layer 2	3.6 %	
Layer 3	4.1 %	
Layer 4	4.3 %	
Total Single		15.4 %
Two or more		3.8 %

As for triggering purpose a coincidence of at least three cell measurements out of four is re-

quired, the trigger inefficiency of a quadruplet is determined by the fraction of times that a δ-ray affects two or more measurements.

From the displayed results we can conclude that while 20% of the tracks produces a δ-ray, only for 3.8% of the tracks two or more layers are affected, spoiling the trigger capability of a single quadruplet.

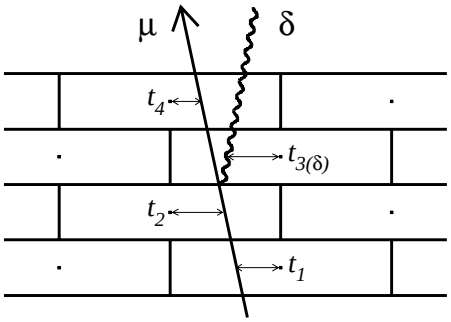

Figure 9. Picture of δ-ray effect : a δ-ray, produced by a crossing μ, affects the drift time t_3

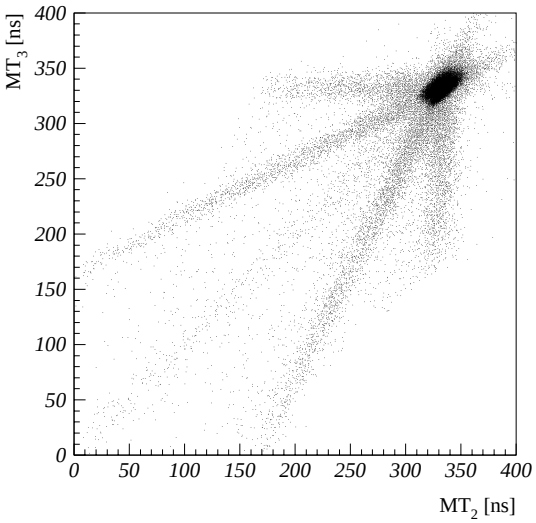

Figure 10. MT_2 versus MT_3. With the definition $MT_j = (t_{j-1} + t_{j+1})/2 + t_j$

8. Drift Velocity

The drift velocity has been calculated for each event as a third parameter in the linear fit of four hits tracks. The tracks with four hits are fitted with a straight line, leaving as a free parameter in the fit the space-time relationship, assuming the nominal position for the wires.

The results are stable and uniform, the distribution of the values calculated for a given configuration of the chamber being gaussians with a r.m.s. compatible with the intrinsic resolution of the cells.

Fig. 11 shows the peak values of the above distributions, obtained for various voltage settings. Their variation is as expected from the simulations. A mean drift velocity of 5.63 cm/μs is obtained for the chamber at the reference setting.

The variation of the apparent drift velocity as a function of the incident angle of the tracks have been studied. The behaviour is as expected : a variation of the average drift velocity is observed on the transverse plane, while there is no effect on the longitudinal plane (fig 12).

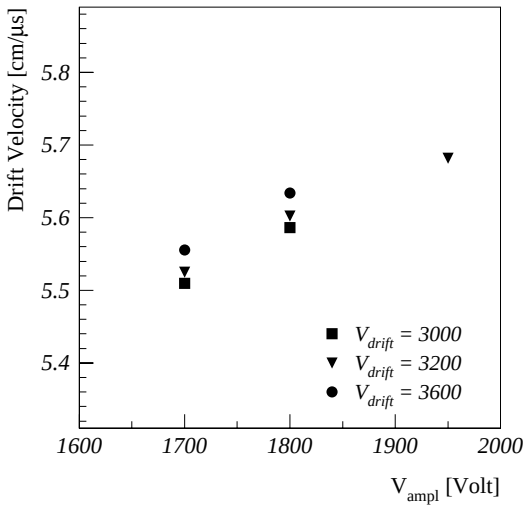

Figure 11. Drift Velocities measured at different voltage settings

The effects of the magnetic field on the drift velocity have been studied : while a component orthogonal to the wires has the effect calculated from the Lorentz angle, which can be easily corrected for, a component along the wire induces distorsions on the drift lines (fig. 3) which has serious implications to the systematic effects due to the different angles of incidence of the tracks.

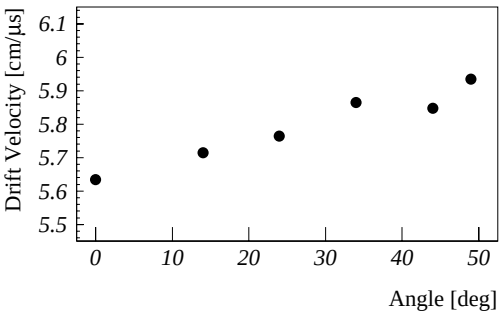

Figure 12. Apparent drift velocities measured for different orthogonal incident angles

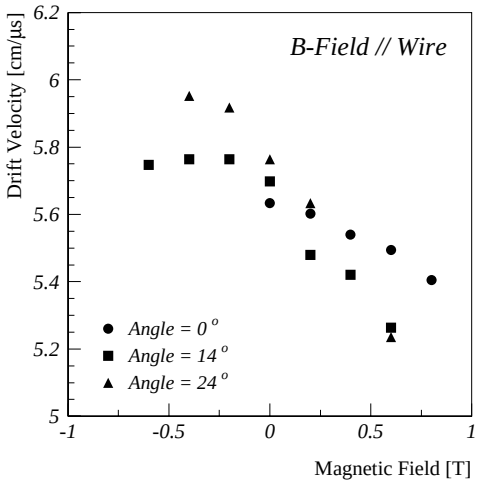

Figure 13. Drift velocities measured for different orthogonal incident angles with different values of the magnetic field

Fig. 13 shows the drift velocities measured for various values of the magnetic field along the wires and the angle of incidence of the tracks. The negative values of the magnetic field in the plot have to be read as effects on tracks with negative incident angles.

The variation of the drift velocity with the incident angle of the tracks and with the magnetic field can be corrected for the track measurement, while it can generate systematic effects on the trigger efficiency, as the trigger processor have to be programmed for a given drift velocity, with few percent tolerance. A carefull optimisation of the trigger processor, depending on its positioning in the CMS detector, is thus needed. Refer to [6] for a preliminary study, based on simulations, of such effects.

9. Linearity

One of the most important features required to the chamber for the triggering with the Mean Timer method is a linear space-time relationship along the full drift space. Such relationship has been calculated from the drift time distribution.

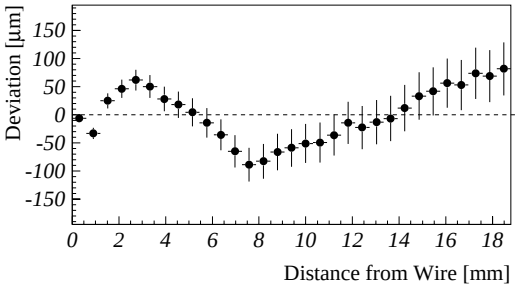

Figure 14. Systematic deviation from linear space-time relationship

The space-time relation of each half-cell, has been fitted with a straight line, and the deviation from the resulting linear behaviour has been measured at each point and converted to μm, assuming a constant and average drift velocity.

Fig. 14 shows the systematic deviation from the

linearity, obtained as the mean deviation among the various half-cells : the non-linearity is everywhere well within 150 μm, below the intrinsic cell resolution.

The behaviour is in agreement with the GARFIELD simulations.

10. Resolution

The position resolution of the cell has been measured as the residual of each single point from a linear fitting performed to a 4 drift times measurement track. No corrections for the non-linearity have been applied.

Fig. 15 shows the mean cell resolutions obtained at various voltages and threshold settings for orthogonally incident tracks. The values are well within the specification required to the single cell resolution for the track measurement.

The resolutions evaluated at different positions along the drift space of the cell for different incident angles are shown in fig. 16. The values are uniform along the full drift space for a wide range of incident angles, while the small worsening of the resolution observed for large angles does not affect the whole performance of the track measurement.

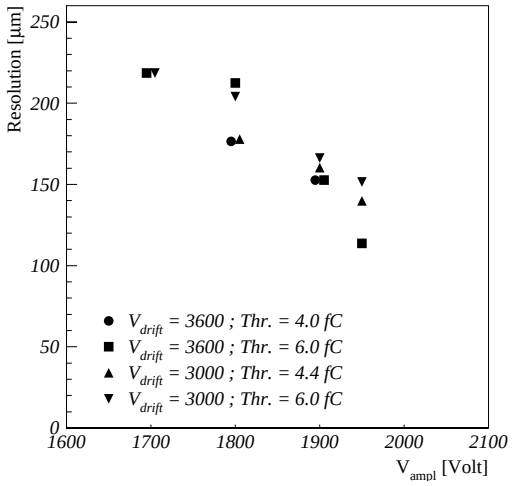

Figure 15. Single point resolution evaluated at different voltages settings for orthogonally incident tracks

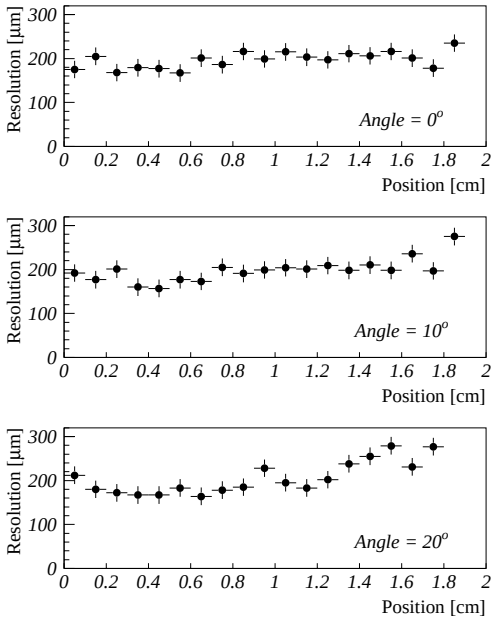

Figure 16. Single point resolution evaluated at different positions along the cell drift space for different incident angles

REFERENCES

1. CMS Technical Proposal, CERN/LHCC 94-38, LHCC/P1, 15 December 1994.
2. F. Gasparini et al., Nucl. Instr. and Meth., A336 (1993) 91.
3. G. Barichello et al., Nucl. Instr. and Meth., A360 (1995) 507.
4. R. Veenhof, *GARFIELD, a Drift Chamber Simulation Program User's Guide*, Version 5.13, CERN Program Library W5050, 1995.
5. F.M. Newcomer et al., IEEE Trans. on Nucl. Sci., 40 (1993) 630.
6. M. De Giorgi et al., Proceedings of the First *Workshop on Electronics for LHC Experimets*, CERN/LHCC 95-56, p.222